Gas-phase reaction between calcium monocation and fluoromethane: Analysis of the potential energy hypersurface and kinetics calculations

Adrián Varela-Álvarez, V. M. Rayón, P. Redondo, C. Barrientos, and José A. Sordo

Related Articles

Additional information on J. Chem. Phys.

Journal Homepage: http://jcp.aip.org/

Journal Information: http://jcp.aip.org/about/about_the_journal

Top downloads: http://jcp.aip.org/features/most_downloaded

Information for Authors: http://jcp.aip.org/authors

Gas-phase reaction between calcium monocation and fluoromethane: Analysis of the potential energy hypersurface and kinetics calculations

Adrián Varela-Álvarez,[1] V. M. Rayón,[2] P. Redondo,[2] C. Barrientos,[2] and José A. Sordo[1,a)]

[1]*Departamento de Química Física y Analítica, Laboratorio de Química Computacional, Facultad de Química, Universidad de Oviedo, Julián Clavería, 8. 33006 Oviedo, Principado de Asturias, Spain*
[2]*Departamento de Química Física y Química Inorgánica, Facultad de Ciencias, Universidad de Valladolid, 47005 Valladolid, Spain*

The gas-phase reaction between calcium monocation and fluoromethane: $Ca^+ + CH_3F \rightarrow CaF^+ + CH_3$ was theoretically analyzed. The potential energy hypersurface was explored by using density functional theory methodology with different functionals and Pople's, Dunning's, Ahlrichs', and Stuttgart–Dresden basis sets. Kinetics calculations (energy and total angular momentum resolved microcanonical variational/conventional theory) were accomplished. The theoretically predicted range for the global kinetic rate constant values at 295 K $(7.2 \times 10^{-11} - 5.9 \times 10^{-10}$ cm^3 molecule^{-1} s$^{-1})$ agrees reasonably well with the experimental value at the same temperature $[(2.6 \pm 0.8) \times 10^{-10}$ cm^3 molecule^{-1} s$^{-1}]$. Explicit consideration of a two transition state model, where the formation of a weakly bounded prereactive complex is preceded by an outer transition state (entrance channel) and followed by an inner transition state connecting with a second intermediate that finally leads to products, is mandatory. Experimental observations on the correlation, or lack of correlation, between reaction rate constants and second ionization energies of the metal might well be rationalized in terms of this two transition state model. © *2009 American Institute of Physics.* [doi:10.1063/1.3247287]

I. INTRODUCTION

Selective metal-mediated activation of carbon-halide bonds is an active research field in organometallic chemistry.[1] Particularly carbon-fluorine bond activation attracts a great deal of interest as a consequence of the adverse influence of fluorocarbons and mixed fluorohalocarbons in the mechanisms of stratospheric ozone depletion[2] or as green-house gases.[3]

From a systematic research on lanthanide cations C–F activation, Heinemann *et al.*[4] and Cornehl *et al.*[5] postulated the single-electron transfer (SET) as the mechanism through which such reactions proceed

$$M^{\bullet+} + R\text{-}F \rightarrow M^{\bullet+} \cdots F\text{-}R \rightarrow M^{2+} \cdots F^- \cdots R^\bullet$$
$$\rightarrow MF^+ + R^\bullet. \quad (1)$$
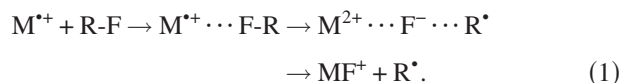
The main evidence supporting such a "harpoon"-like activation mechanism is the correlation found between the second ionization energy (IE) and the overall observed ability of the "bare" lanthanide cations to activate the C–F bond.[5]

Alternatively, formation of $MF^+ + R^\bullet$ products might well proceed through an oxidative addition mechanism[4]

$$M^{\bullet+} + R\text{-}F \rightarrow R^\bullet\text{-}M^+\text{-}F \rightarrow MF^+ + R^\bullet. \quad (2)$$

However, the electronic structures of cations like Ca^+ are not expected to be suitable because reaction (2) formally requires the presence of at least two valence electrons in the metal.

For the case of less reactive cations, such as, for example, Cr^+ cation with a d^5 electronic configuration, Cornehl *et al.*[6] proposed that bond activation proceeds by single coordination of the chromium cation. Thus Cr^+ activates up to four C–F bonds [the first one is schematized in Eq. (3)] in hexafluoroacetane, making them susceptible to hydrolysis[6]

$$CrC_3F_6O^+ + H_2O \rightarrow CrC_3HF_5O_2^+ + HF. \quad (3)$$

Mazurek and Schwarz[7] recently emphasized that a systematic investigation of the "harpoon"-like mechanism versus coordination is indicated.

With the aim of checking the suitability of the SET harpoon-like mechanism, Harvey *et al.*[8] reported the results of a joint theoretical and experimental study on the $Ca^+ + CH_3F \rightarrow CaF^+ + CH_3$ reaction. The main conclusions in that study can be summarized as follows: (a) density functional theory (DFT),[9] through rather popular functionals, such as Slater–Vosko–Wilk–Nusair local spin density approximation functional,[10] Becke–Lee–Yang–Parr (BLYP) generalized gradient approximation (GGA) functional,[11,12] or even the widely employed Becke-3-parameter Lee–Yang–Parr (B3LYP) hybrid GGA functional,[11,12] are unable to properly model the studied reaction. This conclusion warned us about the reliability of some theoretical results on the $M^+ + CH_3F$ reactions employing these types of functionals.[1,13–15] Indeed, the tendency of the DFT(B3LYP) methodology to underestimate reaction barriers is well documented,[16] and (b) although the theoretical exploration of the potential energy surface (PES) and the analysis in terms of the valence bond theory strongly suggest that an harpoon-like mechanism operates, there is no a single correlation between IE(M^+) and reactiv-

a)Electronic mail: jasg@uniovi.es.

ity, which indicates that the mechanism through which metal-mediated activation of carbon-halide bonds is not fully understood yet.

Bearing in mind that Zhao *et al.*[17] recently reported rate coefficients from inductively coupled plasma/selected-ion flow tube experiments for the reactions of methyl fluoride with a number of atomic cations involving fourth-, fifth-, and sixth-period atomic cations (including Ca$^+$), we planned a systematic theoretical research combining the characterization of the PESs for the M$^+$+CH$_3$X (X=H,F,Cl) reactions, followed by kinetics calculations allowing us to compute rate constants to be compared with the experimental data available. We do believe that such a systematic study should provide valuable mechanistic information on the studied processes.

As a preliminary step in the above described project, we need: (a) to show that the PESs for the M$^+$+CH$_3$X reactions can be quantitatively described through practical theoretical methodologies, i.e., levels of theory requesting affordable computational costs, and (b) to confirm that the chosen level of theory is able to provide suitable kinetics information, i.e., rate constants consistent with the experimental values.

It should be noted that Harvey *et al.*[8] showed that the CCSD(T) method represents an appropriate level of theory for the Ca$^+$+CH$_3$F reaction. However, systematic CCSD(T) calculations on reactions involving fourth-, fifth-, and sixth-period atomic cations in order to explore the PESs and subsequent minimum energy path calculations within the context of the variational transition state theory (see below), do not represent a practical theoretical level at all.

In this article we present a DFT theoretical study on the Ca$^+$+CH$_3$F reaction, using different functionals as well as basis sets from several laboratories. Kinetics calculations within the framework of the statistical theories have also been carried out employing several PESs chosen from among those generated at different theoretical levels. We will show that an appropriate choice of the theoretical model leads to kinetics predictions in good agreement with the experimental data available for the studied reaction.

II. METHODS

A. Electronic structure calculations

The PES of the Ca$^+$+CH$_3$F$\rightarrow$CaF$^+$+CH$_3$ reaction was fully explored at the DFT level using several functionals and different basis sets. A preliminary exploration at the Moller–Plesset second order perturbation theory (MP2) level confirmed that, as Harvey *et al.*[8] remarked, it is not an appropriate methodology to be employed as some of the chemically significant structures could not be located on the corresponding PES.

The B3LYP,[11,12] modified Perdew–Wang-1-parameter-method for kinetics (MPW1K),[18] modified Perdew–Wang–Becke-1-parameter-method for kinetics (MPWB1K),[19] and Boese–Martin for kinetics (BMK)[20] functionals were employed. B3LYP, probably the most widely used functional, is a hybrid GGA functional that has been chosen as a reference. We wanted to assess how its reported bad performance for the process under study[8] affects kinetics predictions.

MPW1K and MPWB1K are hybrid and hybrid meta-GGA functional, respectively, that have been optimized against a representative benchmark kinetics database and were found to provide a very good performance for kinetics.[21] Finally, BMK is a hybrid meta-GGA functional specially developed for the exploration of reaction mechanisms. Boese and Martin[20] claimed that, unlike other functionals, the improved accuracy in the calculation of transition state barriers with BMK does not come at the expense of equilibrium properties. Further theoretical details on the characteristics of the above mentioned DFT functionals can be found in a recent review article.[22]

Regarding basis sets, following recommendations on the role of basis sets in DFT calculations,[23] we employed Pople's 6-311+G(2df,2p),[24] Dunning's aug-cc-pVTZ,[25] and Ahlrichs' TZVPP (Ref. 26) triple-zeta quality bases. We also decided to carry out calculations with Dunning's aug-cc-pVDZ double-zeta quality basis set[25] in order to assess the ratio quality/cost when passing from double-zeta to triple-zeta basis sets. This can be a determinant factor to be taken into account in future research when studying reactions involving much more computationally demanding lanthanide cations.[17] Also, bearing in mind such future studies, we have carried out in a parallel way all-electron calculations [using 6-311+G(2df,2p) and TZVPP basis sets] together with calculations employing an effective core potential (ECP) for representing the cationic metal [using 6-311+G(2df,2p) and aug-cc-pVXZ (X=D,T) basis sets]. The Stuttgart–Dresden (SDD) ECP (Ref. 27) was chosen.

The thermodynamic functions (ΔH, ΔS, and ΔG) were estimated within the ideal gas, rigid rotor, and harmonic oscillator approximations.[28] A temperature of 298 K and a pressure of 1 atm were assumed.

All the electronic structure and statistical thermodynamics calculations were performed with the GAUSSIAN 03 package of programs.[29] Geometry optimizations were carry out using a tight convergence criteria and an ultrafine grid for numerical integrations.

B. Kinetics calculations

As we will show, the energy profile for the reaction considered in this work is the one depicted in
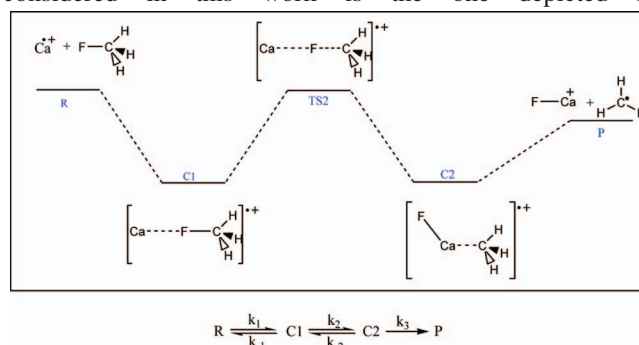
Scheme 1 (energy profile for the Ca$^+$+CH$_3$F$\rightarrow$CaF$^+$+CH$_3$ reaction; energies can be found in Tables IV–VI). Some time ago, Mozurkewich and Benson[30] developed a kinetic theoretical background to deal with this type of processes within the context of the Rice–Ramsperger–Kassel–Marcus (RRKM)

theory.[31–34] The main assumption in Benson–Mozurkewich model is that the pressure is sufficiently low that the intermediates do not undergo any collisions (collisionless regime with the total energy E and total angular momentum J conserved). This constrain is fully compatible with the experimental conditions employed by Zhao *et al.*[17] to measure the rate constant for the Ca$^+$+CH$_3$F→CaF$^+$+CH$_3$ reaction (P =0.35 Torr) Concentrations of **C1** and **C2** structures are determined by steady state rather than equilibrium conditions.[30,35]

The systems considered in this work exhibit rotational constants fulfilling $A_i > B_i \approx C_i$ and therefore the usual approximation that the molecules be treated as a prolate symmetry top rotor should work well. The rotational energy levels depend on two quantum numbers, J and K, as follows,

$$E_i(J,K) = J(J+1)B_i + (A_i - B_i)K^2. \qquad (4)$$

While J is conserved during the course of the reaction, K needs not be. As a matter of fact, the K-rotor is usually treated as active;[32–34] that is, as forming part of the vibrational degrees of freedom when computing the sum of states, $W_i(E,J)$, functions.

Under steady-state conditions, one obtains for the global (observed) rate constant the expression

$$k_{\text{global}} = \frac{\left(\frac{2\pi\mu k_B T}{h^2}\right)^{-3/2}}{hQ_R} \sum_{j=0}^{\infty} \int_{V_{\max}}^{\infty} dE\, W_1(E,J) \frac{W_2(E,J)W_3(E,J)}{W_2(E,J)W_3(E,J) + W_1(E,J)\left[\frac{1}{3}W_2(E,J) + W_3(E,J)\right]} e^{-E/RT}, \qquad (5)$$

where the $W_i(E,J)$ functions are the sum of states at energy lower than E and angular momentum J corresponding to the different transition structures **TS1**-**TS3** (i=1,3).

We approached the convolution of the K-rotor into vibrational sums of states as follows,

$$W_i(E,J) = \sum_{K=0}^{J} W_i(E,J,K) = \sum_{K=0}^{J} g_{JK} W_i(E_i',0,0), \qquad (6)$$

with $E_i' = E - E_i(J,K)$. g_{JK} is the degeneracy associated to the rotational level (JK) [i.e., $2J+1$ if K=0 and $2(2J+1)$ if $K >0$] and $W_i(E_i',0,0)$ represents the sum of active states with $J=K=0$ and energy between the transition state barrier TS$_i$ and E_i'. $V_{\max}$ is the largest value from among the energy barriers associated to **TS1**, **TS2**, or **TS3** in Scheme 1, and Q_R represents the product of the partition functions of reactants, where the center of mass motion partition function, $(2\pi\mu k_B T/h^2)^{3/2}V$, has been factored out [T and V are temperature and volume; R, k_B, and h are gas, Boltzmann and Planck constants, and μ is the reduced mass: $m_{\text{Ca}+}m_{\text{CH3F}}/(m_{\text{Ca}+}+m_{\text{CH3F}})$]. Factor 1/3 affecting $W_2(E,J)$ in the denominator of Eq. (5) corresponds to the reaction symmetry factor associated to the $k_{-2}(E,J)$ rate constant (see Scheme 1).

In the case of processes where no transition structure (first-order saddle point) was found, such as the entrance (**TS1**) and exit (**TS3**) channels (see Scheme 1), the microcanonical variational transition state theory (μVTST) in its vibrator formulation[36,37] was employed. For this purpose, a distinguished-coordinate path (DCP)[38,39] was constructed for each channel. The DCP of the entrance channel was defined as the minimum energy structures found at 95 values of the F–Ca distance in the range 160–3.5 Å. The huge amplitude of this interval was dictated by the fact that the radical-cation interaction has very long range effects according to our calculations. The DCP of the exit channel was defined as the minimum energy structures found at 26 values of the Ca–C distance in the range 15–4.0 Å. Appropriate distributions for the selected points at different regions of the DCP were produced.

We detected that for a few points along the DCP, one (or even two, in some special cases) from among the lower vibrational frequencies became imaginary. An efficient and straightforward way to dealing with that pitfall was to correct frequencies by means of linear interpolations.[40] The problem was observed to occur more often in the case of the BMK functional. As a matter of fact, we do believe that some discrepancies with the rest of functionals, detected when computing the BMK entrance channel (see next section) should be ascribed to the unreliable frequencies predicted along the BMK DCP. $W_i(E,J)$ functions were computed by means of Forst algorithm,[32] using the appropriate frequencies and moments of inertia for the transition states.

The kinetics calculations were carried out by using software implemented by us, which represents a modified version of computer codes we recently employed in a systematic mechanistic study on the N(^{2}D,^{4}S)+CH$_2$X(X=H,F,Cl,Br) reactions.[41] Such codes were originally developed by M. Aschi at the Universitá di L'Aquila.

III. RESULTS AND DISCUSSION

A. Analysis of the PES

Figure 1 depicts the geometries corresponding to the chemically meaningful structures located on the PES and Tables I–III collect the most significant geometrical parameters. Tables IV–VI contain the adiabatic potential energies ($\Delta U_0 = \Delta U$ + zero-point energy correction) and the Gibbs free energies (ΔG) for all the structures as computed with the
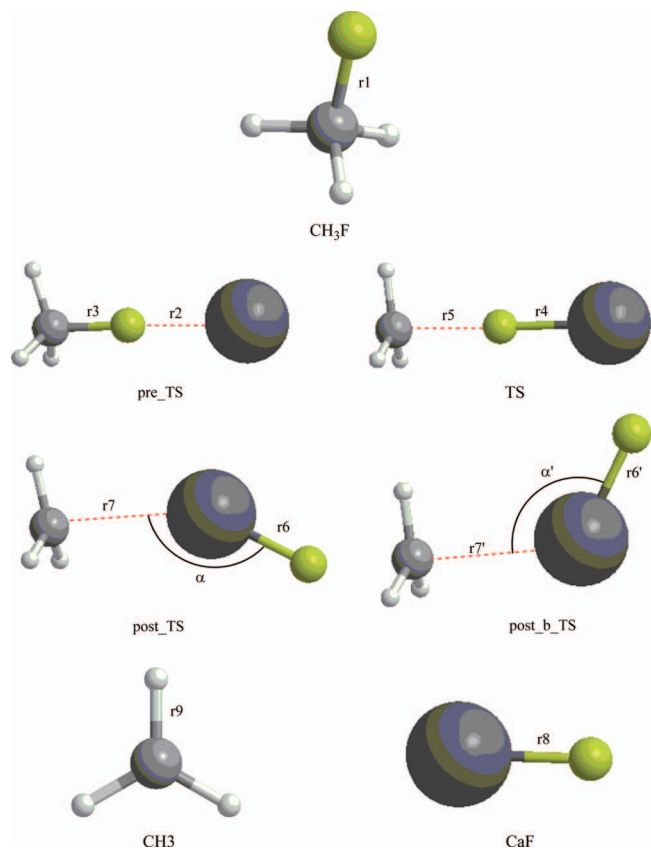
FIG. 1. Structures located on the PES for the $Ca^+ + CH_3F \rightarrow CaF^+ + CH_3$ reaction. Values for the most representative geometrical parameters (r1–r9 and α), as estimated at the different levels of theory employed, are collected in Tables I–III.

different methodologies we employed, and Scheme 1 shows the qualitative energy profile arising from our calculations.

Reaction starts with the barrierless approximation of calcium cation to the fluorine atom in CH_3F, giving rise to a rather stable structure **C1** that, passing through **TS2** transition structure, gives rise to a second intermediate **C2** in which fluorine and calcium atoms are bonded and the latter keeps interacting with the carbon atom of the CH_3 species. Such an interaction becomes weaker and weaker and one then obtains the final products of the reaction, namely, $FCa^+ + CH_3$, through a barrierless endergonic process. A

TABLE II. Most representative geometrical parameters for the $Ca^+ + CH_3F$ $\rightarrow CaF^+ + CH_3$ reaction as estimated with different functionals and Dunning's aug-cc-pVTZ (aug-cc-pVDZ) basis sets. (SDD basis set was employed for Ca in all cases.) Distances are given in angstroms and angle in degrees.

	B3LYP	BMK	MPWB1K	MPW1K
r1	1.392 (1.401)	1.375 (1.387)	1.366 (1.377)	1.367 (1.378)
r2	2.199 (2.207)	2.218 (2.230)	2.202 (2.213)	2.205 (2.213)
r3	1.467 (1.478)	1.442 (1.456)	1.431 (1.443)	1.432 (1.445)
r4	2.016 (2.017)	2.005 (2.005)	1.990 (1.994)	1.996 (1.999)
r5	1.948 (1.955)	2.057 (2.062)	1.962 (1.969)	1.941 (1.948)
r6	1.889 (1.888)	1.897 (1.896)	1.877 (1.878)	1.876 (1.877)
r7	2.784 (2.817)	2.732 (2.742)	2.738 (2.809)	2.754 (2.802)
α	108.4 (122.0)	99.2 (99.8)	100.1 (125.2)	107.4 (124.5)
r8	1.872 (1.871)	1.883 (1.881)	1.860 (1.861)	1.860 (1.860)
r9	1.078 (1.088)	1.079 (1.090)	1.072 (1.081)	1.074 (1.082)

transition structure connecting two equivalent rotamers **C2**, through a rotation around the Ca–C axis, was also located. In any case, this process does not play any role in the global kinetics. Accordingly, data corresponding to this transition structure were not included in Tables I–VI.

Tables I–III plainly show that the different levels of theory employed do predict quite similar geometrical parameters. The only exception corresponds to the α angle in structure **C2** for which noticeable discrepancies sometimes appear (see Table I). However, they must be ascribed to the extreme flatness of the PES, regarding the F–Ca–C (α) angle.

Regarding energetics, Tables IV–VI show that B3LYP tends, in general, to predict greater exergonicities and lower barriers than the rest of functionals. Particularly, the B3LYP barrier associated to **TS2** (see Table VI) is severely underestimated (-6.1 kcal/mol, using TZVPP basis set) when compared with the rest of functionals (from $+4.0$ to $+4.6$ kcal/mol, using TZVPP basis set). Another general trend suggested by data in these tables is that MPW1K predicts higher exergonicities than the other functionals for **C2** and products.

Nevertheless, with the above exceptions in mind, the general conclusion is that all levels of theory employed in the present study do provide energy predictions reasonably

TABLE I. Most representative geometrical parameters (r1–r9 and α; see Fig. 1 for notation) for the $Ca^+ + CH_3F \rightarrow CaF^+ + CH_3$ reaction as estimated with different functionals and Pople's 6-311+G(2df,2p) basis set. (SDD basis set was also was employed for Ca, as indicated in the corresponding table columns.) Distances are given in angstroms and angle in degrees.

	B3LYP (SDD)	B3LYP	BMK (SDD)	BMK	MPWB1K (SDD)	MPWB1K	MPW1K (SDD)	MPW1K
r1	1.390	1.390	1.374	1.374	1.365	1.365	1.365	1.365
r2	2.219	2.226	2.240	2.249	2.226	···	2.225	2.229
r3	1.465	1.465	1.440	1.441	1.431	···	1.432	1.431
r4	2.024	2.030	2.014	2.016	2.000	···	2.005	2.007
r5	1.965	1.940	2.078	2.045	1.981	···	1.959	1.939
r6	1.895	1.888	1.903	1.898	1.887	1.877	1.886	1.874
r7	2.810	2.793	2.743	2.742	2.816	2.748	2.820	2.762
α	121.6	104.1	99.8	95.0	148.6	96.8	150.0	102.7
r8	1.878	1.871	1.888	1.883	1.827	1.860	1.866	1.858
r9	1.078	1.078	1.080	1.080	1.072	1.072	1.073	1.073

TABLE III. Most representative geometrical parameters for the Ca$^+$+CH$_3$F→CaF$^+$+CH$_3$ reaction as estimated with different functionals and Ahlrichs' TZVPP basis set. Distances are given in angstroms and angle in degrees.

	B3LYP	BMK	MPWB1K	MPW1K
r1	1.388	1.373	1.364	1.365
r2	2.230	2.248	2.236	2.235
r3	1.464	1.441	1.430	1.430
r4	2.032	2.019	2.004	2.010
r5	1.953	2.062	1.973	1.950
r6	1.898	1.908	1.888	1.885
r7	2.777	2.725	2.731	2.737
α	102.8	95.2	97.6	101.8
r8	1.882	1.893	1.871	1.869
r9	1.078	1.079	1.072	1.074

consistent. Thus, the exergonicity (and adiabatic potential energy ΔU_0) predicted for **C1** ranges from −15.4 (ΔU_0=−21.5) to −18.0 (ΔU_0=−24.0) kcal/mol and the **TS2** barrier height oscillates between 2.0 (ΔU_0=−3.6) and 4.6 (ΔU_0=−1.1) kcal/mol (leaving apart the B3LYP prediction that, as mentioned above, is notably lower). These latter values agree rather well with the CCSD(T) prediction (ΔU_0=−2.2 kcal/mol) and the experimental estimate (ΔU_0=± 3 kcal/mol).[8]

Consequently, the rather pessimistic conclusion by Harvey *et al.*[8] that DFT is unable to model the Ca$^+$+CH$_3$F→CaF$^+$+CH$_3$ reaction should be tempered. Indeed, our calculations demonstrate that the use of appropriate functionals, specially developed to properly describe thermodynamics and kinetics of chemical processes, like the ones chosen by us (MPW1K, MPWB1K, and BMK), opens the possibility for the use of the less computationally expensive DFT methodology to be systematically extended to reactions involving heavier elements for which experimental data are available and where the use of more computationally demanding methods, such as CCSD(T), becomes prohibitive.[17]

On the other hand, as far as basis sets concerns, there is a reasonable agreement between all-electron and ECP energy predictions as can be confirmed by inspection of entries in Table IV. In fact, the maximum discrepancy observed corresponds to the MPW1K functional (3.5 kcal/mol). This is a

rather satisfactory result that supports the use of ECPs in the study of heavier cations for which existence of reliable all-electron basis sets are somewhat limited.

The 6-311+G(2df,2p) and TZVPP triple-zeta valence quality energy predictions are very similar with a maximum deviation of 1.7 kcal/mol (corresponding to **P**) in the case of MPW1K and BMK functionals. Furthermore, Table V shows that the double-zeta predictions, using Dunning's augmented basis sets, represent an excellent approach to the triple-zeta values with discrepancies lower than about 1 kcal/mol.

From the above analysis one can reach the encouraging conclusion that the use of double-zeta basis sets together with ECPs for the metal cation and modern functional like MPW1K, MPWB1K, or BMK, specially designed to provide a balanced description of thermodynamics and kinetics in chemical reactions, will allow for future systematic researches on the kind of processes considered in this work, covering metal cations from the whole Periodic Table.

B. Analysis of the kinetics results

The energy profile of the process under study (see Scheme 1) is the typical one for gas-phase reactions involving negative activation energies and curved Arrhenius plots as a consequence of the formation of an intermediate complex (**C1**) along the entrance channel[30] connected to a saddle point (**TS2**) with a negative energy with respect to reactants ("inner" transition state).[42] There is also a second intermediate on the PES (**C2**) but it is kinetically much less important (see below).

The presence of an intermediate at the entrance channel implies the existence of an "outer" transition state[42] (**TS1**) at large separations, connecting reactants and **C1**. According to Greenwald *et al.*,[42] consideration of both transition states are required to provide reliable kinetics predictions on these reactions. On the other hand, these authors[43] also emphasized the fact that a canonical implementation of transition state theory, where the intermediates **C1** and **C2** are assumed to have a thermal distribution, is essentially incorrect. The variational minimizations at the E,J-resolved level (microcanonical implementation) is required to provide an appropriate theoretical background.

TABLE IV. 6-311+G(2df,2p) energy predictions in kcal/mol [ΔU_0=ΔU+zero-point energy correction and Gibbs ΔG values calculated considering 1 atm and 298.15 K] using different DFT functionals, for the structures located on the PES of the Ca$^+$+CH$_3$F→CaF$^+$+CH$_3$ reaction. All-electron and ECP (SDD) basis sets were employed.

	B3LYP (SDD)		B3LYP		BMK (SDD)		BMK		MPWB1K (SDD)		MPWB1K[a]		MPW1K (SDD)		MPW1K	
	ΔU_0	ΔG	ΔU_0	ΔG	ΔU_0	ΔG	ΔU_0	ΔG	ΔU_0	ΔG	ΔU_0	ΔG	ΔU_0	ΔG	ΔU_0	ΔG
R	0.0	0.0	0.0	0.0	0.0	0.0	0.0	0.0	0.0	0.0	0.0	0.0	0.0	0.0	0.0	0.0
C1	−24.0	−18.0	−23.7	−17.7	−22.1	−15.9	−21.5	−15.4	−23.0	−17.0	⋯	⋯	−22.7	−16.7	−22.5	−16.5
TS2	−12.3	−6.5	−12.6	−6.8	−1.4	4.3	−2.2	3.5	−1.8	4.0	⋯	⋯	−1.9	3.9	−2.5	3.3
C2	−37.1	−34.9	−39.0	−35.3	−31.1	−27.4	−33.4	−29.0	−32.9	−27.5	−34.3	−30.1	−36.1	−31.6	−38.3	−34.6
P	−23.3	−24.9	−26.4	−28.0	−18.2	−19.8	−21.4	−23.0	−19.7	−21.3	−21.6	−23.3	−22.5	−24.1	−25.9	−27.6

[a]C1 and TS2 structures (see Fig. 1) were not located on the PES at this level of theory.

TABLE V. aug-cc-pVTZ (aug-cc-pVDZ) energy predictions in kcal/mol [$\Delta U_0 = \Delta U +$ zero-point energy correction and ΔG values calculated considering 1 atm and 298.15 K] using different DFT functionals for the structures located on the PES of the $Ca^+ + CH_3F \rightarrow CaF^+ + CH_3$ reaction.

	B3LYP (SDD)		BMK (SDD)		MPWB1K (SDD)		MPW1K (SDD)	
	ΔU_0	ΔG	ΔU_0	ΔG	ΔU_0	ΔG	ΔU_0	ΔG
R	0.0 (0.0)	0.0 (0.0)	0.0 (0.0)	0.0 (0.0)	0.0 (0.0)	0.0 (0.0)	0.0 (0.0)	0.0 (0.0)
C1	−24.6 (−24.0)	−17.9 (−18.1)	−23.3 (−22.2)	−17.1 (−16.0)	−23.5 (−23.0)	−17.4 (−17.1)	−23.1 (−22.8)	−17.1 (−16.9)
TS2	−13.3 (−13.3)	−6.8 (−7.6)	−3.6 (−2.7)	2.0 (2.6)	−2.8 (−3.5)	2.9 (2.0)	−2.8 (−3.7)	2.8 (1.8)
C2	−40.4 (−40.0)	−36.2 (−36.7)	−35.3 (−34.5)	−31.1 (−30.8)	−36.3 (−36.6)	−32.7 (−32.2)	−39.9 (−40.3)	−36.4 (−37.0)
P	−26.9 (−26.1)	−27.8 (−27.7)	−22.2 (−21.3)	−23.9 (−22.9)	−22.8 (−22.7)	−24.4 (−24.3)	−26.6 (−26.7)	−28.2 (−28.3)

Table VII collects the values, at different temperatures, for the global kinetic rate constant (k_{global}) and its limiting behavior when the tighter inner transition state provides the dominant bottleneck for the reaction (k_{inner}) or when the looser outer transition state controls the rate constant (k_{outer}) (further values for a wider range of temperatures are provided as supplementary material).[44]

Calculations were carried out for some selected theoretical levels (B3LYP/TZVPP, BMK/TZVPP, MPWB1K/TZVPP, MPW1K/6-311+$G(2df,2p)$+SDD, MPW1K/aug-cc-pVTZ+SDD, and MPW1K/TZVPP) to learn how kinetics predictions do depend on the PES shape. Figure 2 shows the corresponding plots. In order to assess the limitations of the canonical approximation in the present case, as well as the drawbacks associated to one transition state (1TS) kinetics models (which do not consider the outer transition state), recently stressed by Greenwald *et al.*[42] and Georgievskii and Klippestein,[43] we also included in Fig. 2 Arrhenius plots for canonical estimates of the global rate constant using 1TS and 3TS models, the latter considering inner, outer, and dissociation transition states.

The different canonical global rate constants were computed according to

$$k_{global,1TS}^{Canonical} = \frac{k_1 k_2}{k_{-1}},$$

$$k_{global,2TS}^{Canonical} = \frac{k_1 k_2}{k_{-1} + k_2}, \quad (7)$$

$$k_{global,3TS}^{Canonical} = \frac{k_1 k_2 k_3}{k_2 k_3 + k_{-1}(k_3 + k_{-2})},$$

where the k_i rate constants were estimated using canonical transition state theory (the corresponding values are provided as supplementary material).[44]

It should be stressed that k_3 (dissociation) is not included in tables and figures because it is so big that its consideration does not affect the computation of k_{global} in Eq. (2) (it is easy to show that high values of $W_3(E,J)$ make k_{global} in Eq. (2) independent of the dissociation process). In this context, it should be mentioned that the $k_{global,3TS}^{Canonical}$ values, reported in Table VII and plotted in Fig. 2, are practically identical to the corresponding $k_{global,2TS}^{Canonical}$ values (see supplementary material) obtained by neglecting the dissociation channel.

From a qualitative viewpoint, most of the Arrhenius plots for the outer and inner components of k_{global} are rather

TABLE VI. TZVPP energy predictions in kcal/mol [$\Delta U_0 = \Delta U +$ zero-point energy correction and Gibbs ΔG values calculated considering 1 atm and 298.15 K] using different DFT functionals for the structures located on the PES of the $Ca^+ + CH_3F \rightarrow CaF^+ + CH_3$ reaction.

	B3LYP		BMK		MPWB1K		MPW1K	
	ΔU_0	ΔG	ΔU_0	ΔG	ΔU_0	ΔG	ΔU_0	ΔG
R	0.0	0.0	0.0	0.0	0.0	0.0	0.0	0.0
C1	−23.5	−17.6	−21.5	−15.4	−22.3	−16.4	−21.9	−16.0
TS2	−11.9	−6.1	−1.6	4.0	−1.1	4.6	−1.1	4.6
C2	−38.0	−34.2	−32.0	−27.8	−33.2	−29.2	−36.9	−33.0
P	−25.3	−26.9	−19.7	−21.3	−20.3	−21.9	−24.3	−25.9

TABLE VII. Kinetic rate constants (see text for definitions), in cm^3 molecule^{-1} s^{-1}, as computed at different temperatures and theoretical levels.

T (K)	B3LYP/TZVPP				BMK/TZVPP				MPWB1K /TZVPP			
	k_{outer}	k_{inner}	k_{global}	$k_{global,3TS}^{Canonical}$	k_{outer}	k_{inner}	k_{global}	$k_{global,3TS}^{Canonical}$	k_{outer}	k_{inner}	k_{global}	$k_{global,3TS}^{Canonical}$
135	7.77×10^{10}	1.26×10^{6}	7.76×10^{10}	7.77×10^{10}	1.26×10^{6}	4.35×10^{10}	4.00×10^{10}	2.09×10^{9}	5.75×10^{10}	1.40×10^{10}	8.03×10^{11}	2.07×10^{10}
215	6.56×10^{10}	5.43×10^{7}	6.54×10^{10}	6.56×10^{10}	4.17×10^{9}	2.65×10^{10}	2.41×10^{10}	4.42×10^{10}	5.39×10^{10}	9.97×10^{11}	7.10×10^{11}	1.03×10^{10}
295	5.94×10^{10}	3.13×10^{7}	5.91×10^{10}	5.94×10^{10}	2.75×10^{9}	2.22×10^{10}	1.97×10^{10}	2.58×10^{10}	5.11×10^{10}	9.53×10^{11}	7.24×10^{11}	8.64×10^{11}
375	5.57×10^{10}	2.06×10^{7}	5.54×10^{10}	5.57×10^{10}	2.08×10^{9}	2.17×10^{10}	1.86×10^{10}	2.16×10^{10}	4.92×10^{10}	1.03×10^{10}	7.85×10^{11}	8.77×10^{11}
455	5.31×10^{10}	1.46×10^{7}	5.27×10^{10}	5.31×10^{10}	1.70×10^{9}	2.27×10^{10}	1.87×10^{10}	2.09×10^{10}	4.78×10^{10}	1.17×10^{10}	8.72×10^{11}	9.53×10^{11}
535	5.10×10^{10}	1.08×10^{7}	5.05×10^{10}	5.10×10^{10}	1.45×10^{9}	2.46×10^{10}	1.94×10^{10}	2.15×10^{10}	4.66×10^{10}	1.35×10^{10}	9.70×10^{11}	1.06×10^{10}
615	4.91×10^{10}	5.06×10^{8}	4.86×10^{10}	4.91×10^{10}	1.27×10^{9}	2.70×10^{10}	2.04×10^{10}	2.25×10^{10}	4.54×10^{10}	1.57×10^{10}	1.07×10^{10}	1.17×10^{10}
695	4.75×10^{10}	5.06×10^{8}	4.68×10^{10}	4.75×10^{10}	1.13×10^{9}	2.98×10^{10}	2.14×10^{10}	2.37×10^{10}	4.42×10^{10}	1.80×10^{10}	1.17×10^{10}	1.28×10^{10}
775	4.60×10^{10}	5.06×10^{8}	4.53×10^{10}	4.59×10^{10}	1.02×10^{9}	3.28×10^{10}	2.24×10^{10}	2.49×10^{10}	4.30×10^{10}	2.05×10^{10}	1.27×10^{10}	1.39×10^{10}
855	4.47×10^{10}	4.07×10^{8}	4.39×10^{10}	4.45×10^{10}	9.31×10^{10}	3.60×10^{10}	2.33×10^{10}	2.60×10^{10}	4.20×10^{10}	2.31×10^{10}	1.37×10^{10}	1.49×10^{10}
935	4.35×10^{10}	3.33×10^{8}	4.26×10^{10}	4.33×10^{10}	8.59×10^{10}	3.93×10^{10}	2.41×10^{10}	2.70×10^{10}	4.09×10^{10}	2.57×10^{10}	1.45×10^{10}	1.58×10^{10}
1015	4.35×10^{10}	2.76×10^{8}	4.14×10^{10}	4.21×10^{10}	7.98×10^{10}	4.27×10^{10}	2.49×10^{10}	2.78×10^{10}	4.00×10^{10}	2.85×10^{10}	1.53×10^{10}	1.66×10^{10}
1095	4.15×10^{10}	2.32×10^{8}	4.04×10^{10}	4.11×10^{10}	7.46×10^{10}	4.61×10^{10}	2.55×10^{10}	2.85×10^{10}	3.91×10^{10}	3.12×10^{10}	1.60×10^{10}	1.74×10^{10}

T (K)	MPW1K/6-311+$G(2df,2p)$+SDD				MPW1K/aug-cc-pVTZ+SDD				MPW1K/TZVPP			
	k_{outer}	k_{inner}	k_{global}	$k_{global,3TS}^{Canonical}$	k_{outer}	k_{inner}	k_{global}	$k_{global,3TS}^{Canonical}$	k_{outer}	k_{inner}	k_{global}	$k_{global,3TS}^{Canonical}$
135	8.67×10^{10}	5.58×10^{10}	2.59×10^{10}	7.65×10^{10}	8.10×10^{10}	2.37×10^{9}	4.83×10^{10}	8.07×10^{10}	8.17×10^{10}	1.41×10^{10}	9.34×10^{11}	2.39×10^{10}
215	7.02×10^{10}	3.19×10^{10}	1.85×10^{10}	3.68×10^{10}	6.79×10^{10}	1.22×10^{9}	3.67×10^{10}	6.26×10^{10}	6.83×10^{10}	9.94×10^{11}	7.62×10^{11}	1.08×10^{10}
295	6.21×10^{10}	2.51×10^{10}	1.60×10^{10}	2.30×10^{10}	6.09×10^{10}	8.66×10^{10}	3.15×10^{10}	4.73×10^{10}	6.12×10^{10}	9.41×10^{11}	7.49×10^{11}	8.83×10^{11}
375	5.74×10^{10}	2.30×10^{10}	1.51×10^{10}	1.86×10^{10}	5.68×10^{10}	7.17×10^{10}	2.89×10^{10}	3.78×10^{10}	5.70×10^{10}	1.01×10^{10}	7.98×10^{11}	8.86×10^{11}
455	5.42×10^{10}	2.29×10^{10}	1.51×10^{10}	1.71×10^{10}	5.39×10^{10}	6.46×10^{10}	2.74×10^{10}	3.26×10^{10}	5.41×10^{10}	1.14×10^{10}	8.76×10^{11}	9.55×10^{11}
535	5.18×10^{10}	2.37×10^{10}	1.53×10^{10}	1.67×10^{10}	5.17×10^{10}	6.13×10^{10}	2.66×10^{10}	2.98×10^{10}	5.18×10^{10}	1.31×10^{10}	9.69×10^{11}	1.05×10^{10}
615	4.97×10^{10}	2.50×10^{10}	1.57×10^{10}	1.69×10^{10}	4.97×10^{10}	6.00×10^{10}	2.60×10^{10}	2.81×10^{10}	4.99×10^{10}	1.51×10^{10}	1.07×10^{10}	1.16×10^{10}
695	4.78×10^{10}	2.67×10^{10}	1.62×10^{10}	1.73×10^{10}	4.80×10^{10}	5.98×10^{10}	2.56×10^{10}	2.72×10^{10}	4.81×10^{10}	1.72×10^{10}	1.17×10^{10}	1.27×10^{10}
775	4.61×10^{10}	2.86×10^{10}	1.67×10^{10}	1.77×10^{10}	4.64×10^{10}	6.05×10^{10}	2.54×10^{10}	2.66×10^{10}	4.66×10^{10}	1.95×10^{10}	1.27×10^{10}	1.38×10^{10}
855	4.46×10^{10}	3.06×10^{10}	1.72×10^{10}	1.82×10^{10}	4.50×10^{10}	6.16×10^{10}	2.52×10^{10}	2.62×10^{10}	4.52×10^{10}	2.19×10^{10}	1.36×10^{10}	1.48×10^{10}
935	4.33×10^{10}	3.27×10^{10}	1.76×10^{10}	1.87×10^{10}	4.37×10^{10}	6.31×10^{10}	2.51×10^{10}	2.59×10^{10}	4.39×10^{10}	2.44×10^{10}	1.44×10^{10}	1.57×10^{10}
1015	4.20×10^{10}	3.49×10^{10}	1.80×10^{10}	1.91×10^{10}	4.25×10^{10}	6.48×10^{10}	2.50×10^{10}	2.57×10^{10}	4.28×10^{10}	2.69×10^{10}	1.52×10^{10}	1.65×10^{10}
1095	4.09×10^{10}	3.71×10^{10}	1.84×10^{10}	1.95×10^{10}	4.15×10^{10}	6.66×10^{10}	2.49×10^{10}	2.56×10^{10}	4.17×10^{10}	2.95×10^{10}	1.60×10^{10}	1.73×10^{10}

similar (see Fig. 3). In all cases k_{outer} varies with temperature in a similar way than that recently reported by Zheng *et al.*[45] for methyl radical association, a prototypical barrierless process; this rate constant becomes lower as the temperature increases. In the case of the BMK functional, the k_{outer} rate constant is sensibly greater (specially at the lower temperatures) than when estimated from the rest of functionals, probably as a consequence of the anomalies observed in the BMK estimate of some of the low frequencies, as was already mentioned in the previous section devoted to describe the kinetics calculations.

On the other hand, k_{inner} exhibits, in most cases, a similar behavior than that recently reported by Georgievskii and Klippenstein[46] for C_2H_6+CN reaction, a radical-molecule reaction with similar energy profile than that shown in Scheme 1 for the Ca$^+$+CH$_3$F reaction, namely, a barrierless process with a negative activation energy. At lower temperatures, k_{inner} decreases with increasing temperature as a direct consequence of the presence of a barrier with an adiabatic potential energy lower than reactants. At a given temperature, the entropy contribution becomes controlling and the usual temperature dependence is recovered. Such a critical temperature varies with the theoretical level employed from about 670 K (MPW1K/aug-cc-pVTZ+SDD) to about

250 K (MPW1K/TZVPP). For the B3LYP functional, the inner barrier becomes so low (see Tables IV–VI) that kinetics is fully controlled by the outer bottleneck (see inset 1 in Fig. 2). The B3LYP k_{inner} values increase with the decreasing temperature.

It is striking, however, that despite the apparent bad performance in the calculation of k_{inner} (with B3LYP) and k_{outer} (with BMK) shown in Fig. 3, the calculated global rate constant, which is the one to be compared with the experimental measurement (see below), does not differ too much from the corresponding values predicted by the rest of functionals, as can be seen in Fig. 2 or by direct inspection of Table VII. This important observation allows us to conclude that special care should be exercised when a good agreement between theoretically estimated and experimentally measured reaction rate constants leads us to conclude that the level of calculation employed is appropriate to provide reliable PESs. As the above mentioned results suggest, consistent kinetics predictions on global rate constants for a given process might well rest sometimes on inaccurate PESs descriptions.

Examination of the different insets in Fig. 2 leads us to the conclusion that, in general, the inner bottleneck controls kinetics although with an appreciable (never negligible) contribution from the outer bottleneck. Of course, B3LYP pre-
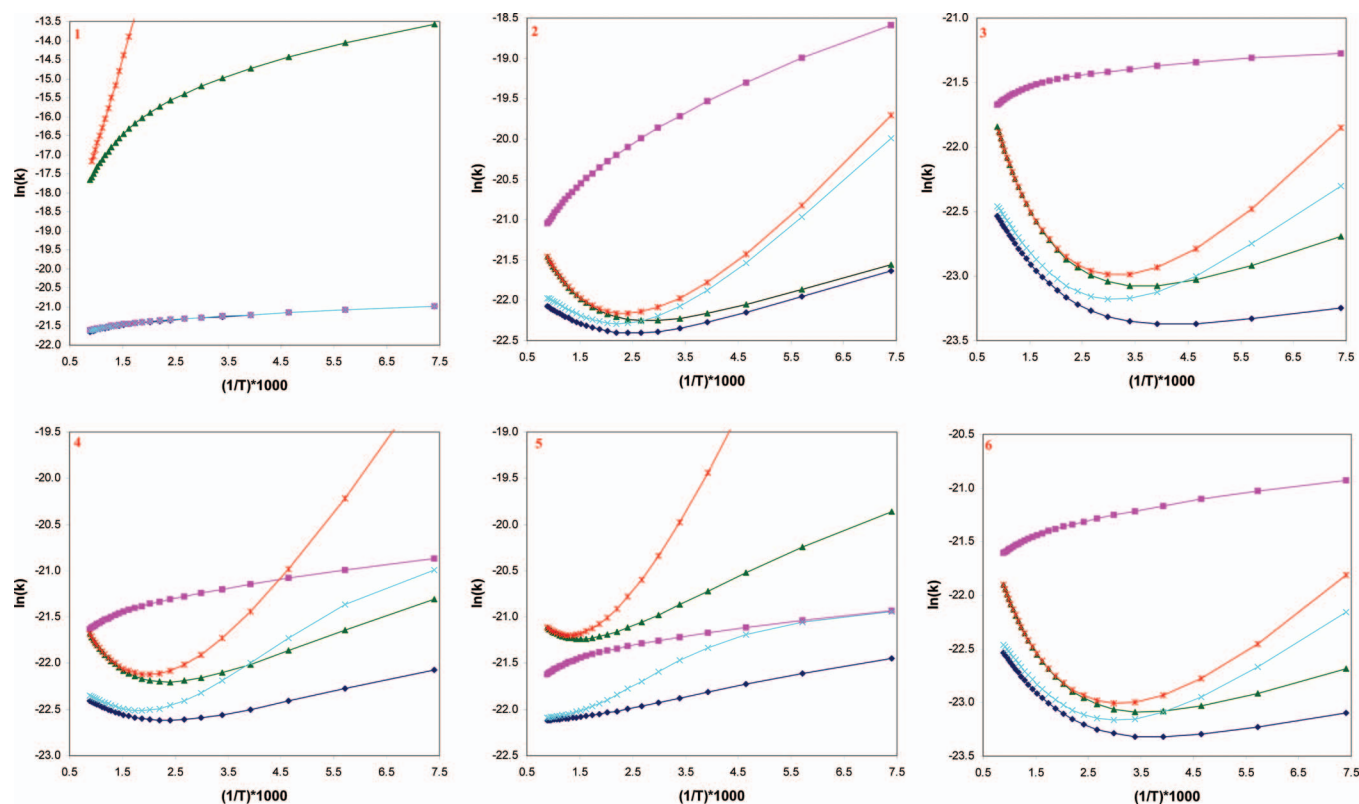
FIG. 2. Arrhenius plots (k is given in cm^3 molecule^{-1} s^{-1} and T in K) for the global rate constant, k_{global} (deep blue line), and its main limiting components (see the text for definitions): k_{inner} (green line) and k_{outer} (pink line). Two canonical estimates of the global rate constant (see the text for details): $k_{global,1TS}^{Canonical}$ (red line) and $k_{global,3TS}^{Canonical}$ (pale blue line) are also depicted. B3LYP/TZVPP (inset 1), BMK/TZVPP (inset 2), MPWB1K/TZVPP (inset 3), MPW1K/6-311 $+G(2df,2p)+$SDD (inset 4), MPW1K/aug-cc-pVTZ+SDD (inset 5), and MPW1K/TZVPP (inset 6).

diction is the exception as a consequence of the already mentioned remarkably low barrier predicted by this functional for the inner (**TS2**) transition state.

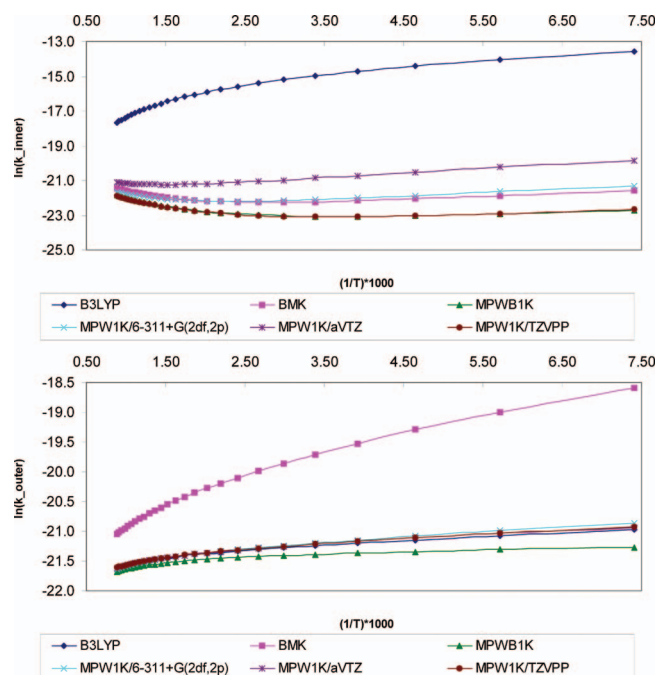In the case of the MPW1K/aug-cc-pVTZ+SDD predic-

FIG. 3. Comparative Arrhenius plots for k_{inner} (upper inset) and k_{outer} (lower inset) as computed at different theoretical levels.

tions, the outer rate constant (**TS1**) becomes smaller at all the temperatures considered. The MPW1K/aug-cc-pVTZ +SDD predicted barrier for **TS2** ($\Delta U_0 = -2.8$ kcal/mol) and global rate constant (3.15×10^{-10} cm^3 molecule^{-1} s^{-1} at 295 K) are fully consistent with their respective experimental estimates, namely, ± 3 kcal/mol,[8] and $[(2.6 \pm 0.8) \times 10^{-10}$ cm^3 molecule^{-1} s$^{-1}]$ at 295 K,[17] respectively. Therefore, from the mechanistic viewpoint, a situation in which both the outer and the inner bottlenecks make appreciable contributions to the global rate constant is totally acceptable. This is a very important point because, as we will show below, the different nature of the inner (**TS2**) and outer (**TS1**) transition states can help rationalize the experimental observations about the type of mechanism (harpoon-like versus oxidative addition)[17] through which reactions of methyl fluoride with metal cations occur. Table VIII collects some virtual data showing limiting behaviors depending on the relative weight of the inner and outer components contributing to k_{global}. Three different values of the **TS2** inner barrier height, relative to reactants, (-5.0, 0.0, and $+5.0$ kcal/mol) are considered. The outer **TS1** barrier was kept fixed and equal to the MPW1K/TZVPP predicted value (the MPW1K/ TZVPP adiabatic inner barrier was -1.1 kcal/mol; see Table VI). When the inner barrier is lower than reactants (-5.0 kcal/mol), k_{global} becomes mostly controlled by the outer bottleneck. If this barrier becomes higher than reactants ($+5.0$ kcal/mol), the inner transition state becomes the controlling bottleneck. In intermediate situations (close to barri-

TABLE VIII. Dependence of the MPW1K/TZVPP global kinetic rate constant values (cm^3 molecule^{-1} s^{-1}) on the relative importance of the outer and inner bottlenecks (adiabatic potential energies of −5.0, 0.0, and +5.0 kcal/mol were assumed for the inner TS2.

T	k_{outer}	$k_{inner}^{\Delta U_0=-5.0}$	$k_{global}^{\Delta U_0=-5.0}$	$k_{inner}^{\Delta U_0=0.0}$	$k_{global}^{\Delta U_0=0.0}$	$k_{inner}^{\Delta U_0=5.0}$	$k_{global}^{\Delta U_0=5.0}$
135	8.17×10^{10}	1.99×10^{8}	7.45×10^{10}	5.73×10^{12}	5.56×10^{12}	4.60×10^{20}	4.60×10^{20}
215	6.83×10^{10}	9.31×10^{9}	6.02×10^{10}	9.92×10^{12}	9.46×10^{12}	8.20×10^{17}	8.18×10^{17}
295	6.12×10^{10}	5.91×10^{9}	5.26×10^{10}	1.60×10^{11}	1.49×10^{11}	3.15×10^{15}	3.14×10^{15}
375	5.70×10^{10}	4.36×10^{9}	4.81×10^{10}	2.42×10^{11}	2.18×10^{11}	2.94×10^{14}	2.91×10^{14}
455	5.41×10^{10}	3.50×10^{9}	4.50×10^{10}	3.46×10^{11}	3.02×10^{11}	1.37×10^{13}	1.35×10^{13}
535	5.18×10^{10}	2.96×10^{9}	4.26×10^{10}	4.72×10^{11}	3.97×10^{11}	4.27×10^{13}	4.17×10^{13}
615	4.99×10^{10}	2.59×10^{9}	4.06×10^{10}	6.18×10^{11}	4.99×10^{11}	1.03×10^{12}	9.96×10^{13}
695	4.81×10^{10}	2.32×10^{9}	3.90×10^{10}	7.82×10^{11}	6.06×10^{11}	2.09×10^{12}	1.99×10^{12}
775	4.66×10^{10}	2.13×10^{9}	3.75×10^{10}	9.61×10^{11}	7.15×10^{11}	3.74×10^{12}	3.50×10^{12}
855	4.52×10^{10}	1.99×10^{9}	3.62×10^{10}	1.15×10^{10}	8.22×10^{11}	6.08×10^{12}	5.60×10^{12}
935	4.39×10^{10}	1.88×10^{9}	3.51×10^{10}	1.36×10^{10}	9.27×10^{11}	9.19×10^{12}	8.31×10^{12}
1015	4.28×10^{10}	1.79×10^{9}	3.42×10^{10}	1.57×10^{10}	1.03×10^{10}	1.31×10^{11}	1.16×10^{11}
1095	4.17×10^{10}	1.73×10^{9}	3.33×10^{10}	1.78×10^{10}	1.12×10^{10}	1.79×10^{11}	1.55×10^{11}

erless), like that predicted by the MPW1K/TZVPP level (−1.1 kcal/mol), a combined kinetic control of the process should be expected. In these latter cases, consideration of a two transition state model is mandatory, in full agreement with recent conclusions by Greenwald *et al.*[42] and Georgievskii and Klippenstein[46] when studying radical-molecule reactions.

Table VII shows that the theoretically predicted range for k_{global} $(7.2 \times 10^{-11}$–5.9×10^{-10} cm^3 molecule^{-1} s^{-1} at 295 K) agrees reasonably well with the experimental value measured at the same temperature [$(2.6 \pm 0.8) \times 10^{-10}$ cm^3 molecule^{-1} s^{-1}].[17] Indeed, it should be mentioned at this point that the theoretical estimation of reaction rate constants is by no means a trivial task. As stressed very recently,[47] relatively small errors in the theoretical estimate of $\Delta G^{\ddagger}$ values do produce considerable deviations in the predicted rate constants. A trivial calculation suggests that an error in about 1 kcal/mol in $\Delta G^{\ddagger}$ (the goal is not always achieved at all in today's theoretical thermodynamic predictions for small-sized systems),[48–53] gives rise to discrepancies close to one order of magnitude in the rate constant. Therefore, despite impressive advances in the accuracy of DFT methodologies accomplished during the last few years,[22] discrepancies between experimentally measured and theoretically predicted rate constants are unavoidable. This important point that have been recently stressed by several authors in different contexts,[47,54–56] should be kept in mind when assessing the output of kinetics theoretical predictions.
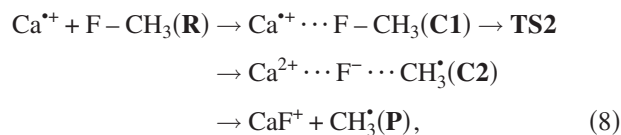
C. Some mechanistic considerations

Before ending, we would like to make some remarks on the mechanism of the Ca$^+$+CH$_3$F→CaF$^+$+CH$_3$ reaction

which should be taken into account when confronting the harpoon-like and the oxidative addition (addition/elimination) mechanisms[8,17] proposed to interpret the experimental data available on this process.

Table IX collects the predicted charges and spin densities on calcium, fluorine, and CH$_3$ species in **C1** and **C2** intermediates, as well as their corresponding values for **TS2** transition structure. They have been computed at the MPW1K/TZVPP level of theory, using Mulliken population analysis (MPA)[57] and Bader's atoms in molecules (AIM) (Ref. 58) methods.

The detailed analysis of data in Table IX plainly suggests a SET harpoon-like mechanism

$$Ca^{\bullet+} + F - CH_3(\mathbf{R}) \rightarrow Ca^{\bullet+} \cdots F - CH_3(\mathbf{C1}) \rightarrow \mathbf{TS2}$$
$$\rightarrow Ca^{2+} \cdots F^- \cdots CH_3^{\bullet}(\mathbf{C2})$$
$$\rightarrow CaF^+ + CH_3^{\bullet}(\mathbf{P}), \quad (8)$$

and therefore **TS2** corresponds to a transition structure where a one electron transfer is carried out from calcium to fluorine. As, according to the kinetics calculations presented in the previous section, **TS2** represents an important contribution to the k_{global} rate constant, it should be expected that in this particular case, the barrier height of **TS2**, and consequently k_{global}, is governed by the value of the second IE of calcium atom.[8] However, for other cases where k_{global} might be controlled by the capture channel (k_{outer}), no correlation with the second IE of the metal should be expected.[17]

We are in the process of applying all the experience gained in the present work to extend our studies to different cations throughout the Periodic Table for which kinetic experimental information is available.[17]

TABLE IX. MPW1K/TZVPP calcium, fluorine (parentheses), and CH$_3$ [brackets] partial charges (au) and spin densities according to Mulliken Population Analysis (MPA) and Bader's Atoms in Molecules (AIM) models.

	Partial charge:		Spin density:	
	MPA	AIM	MPA	AIM
C1	0.936(−0.352)[0.416]	0.999(−0.758)[0.756]	1.002(−0.008)[0.006]	0.950(0.044)[0.006]
TS2	1.216(−0.591)[0.374]	1.345(−0.792)[0.443]	0.579(−0.045)[0.468]	0.523(0.063)[0.416]
C2	1.502(−0.604)[0.102]	1.702(−0.767)[0.063]	0.076(−0.001)[0.925]	0.066(0.001)[0.891]

Regarding the question about the suitability of the canonical kinetic model to study the present reaction, Fig. 2 shows that $k_{\text{global,3TS}}^{\text{Canonical}}$ represents, in general an acceptable approximation to the (E,J)-resolved rate coefficients k_{global} at higher temperatures. As temperature becomes lower and lower, discrepancies appear (for example, at 135 K, the BMK/TZVPP $k_{\text{global,3TS}}^{\text{Canonical}}$ becomes five times greater than k_{global}). As expected, much more severe deviations from k_{global} are predicted by the simple $k_{\text{global,1TS}}^{\text{Canonical}}$ one transition state approximation in the cases where the outer bottleneck becomes the main kinetic controlling factor (see specially insets 1 and 5 in Fig. 2).

IV. CONCLUSIONS

The gas-phase reaction between calcium monocation and fluoromethane: $Ca^+ + CH_3F \rightarrow CaF^+ + CH_3$, was theoretically analyzed by using *ab initio* methodologies and kinetics calculations. Density functional theory with B3LYP, modified MPW1K method for kinetics, modified MPWB1K method, and Boese-Martin for kinetics functionals together with Pople's 6-311+G(2df,2p), Dunning's aug-cc-pVXZ (X=D,T) and Ahlrichs' TZVPP basis sets, and SDD ECPs were employed.

A kinetics microcanonical formulation based on the extension of the RRKM theory was implemented. The dynamics in the region of the prereactive weakly bounded intermediate formed in the entrance channel is supposed to occur in a collision-free environment with total energy and total angular momentum conserved. A two transition state model is adopted: An outer (looser) transition state controlling the entrance channel and an inner transition state located in the neighborhood of the saddle point were considered. A third transition state controlling the exit channel, leading to the final products, does not affect the global rate constant at all.

The theoretically predicted range for the global rate constant values at 295 K (7.2×10^{-11}–5.9×10^{-10} cm^3 molecule^{-1} s^{-1}) agrees reasonably well with the experimental value at the same temperature $[(2.6 \pm 0.8) \times 10^{-10}$ cm^3 molecule^{-1} s$^{-1}]$, bearing in mind the accuracy achieved by the levels of theory computationally affordable at present days to deal with the systems involved in the studied process.

We show that the global rate constant is controlled by the relative values of the outer and inner transition states located on the potential energy hypersurface. The inner transition state represents a one-electron transfer process (harpoon-like mechanism) from the metal cation to the fluorine atom. Thus, when the inner transition state barrier is high as compared with that associated to the outer transition state, the global rate constant will be expected to be governed by the value of the second IE of the metal; the greater the latter the lower the former. In the case that the outer transition state controls the global rate constant, no such correlation should be observed. This considerations might help rationalize the apparently lack of correlation experimentally observed in many cases.

Further studies covering a number of metal cations throughout the Periodic Table are required to confirm this fundamental mechanistic aspect. As shown in the present work, the use of double-zeta valence quality basis sets together with ECPs for the metal cation and DFT functionals specially developed to provide a balanced description of thermodynamics and kinetics in chemical reactions represents an appropriate theoretical level to study this type of processes. Such a methodology results computationally affordable to extend the present study to late-transition metal cations for which abundant kinetic data is presently available. Work in that direction is in progress at our laboratory.

[1] X. Zhao, A. C. Hopkinson, and D. K. Bohme, ChemPhysChem **9**, 873 (2008), and references therein.
[2] "Scientific Assessment of Ozone Depletion 2002," Global Ozone Research Monitoring Report No. 47, C. A. Ennis, Coordinating Editor, WMO, Geneve, Switzerland, 2003.
[3] T. G. Spiro and W. H. Stigliani, *Chemistry of the Environment*, 2nd ed. (Prentice-Hall, Uppon Saddle River, 2003).
[4] C. Heinemann, N. Goldberg, I. C. Tornieporth-Oething, T. M. Klapötke, and H. Schwarz, Angew Chem., Int. Ed. Engl. **34**, 213 (1995).
[5] H. H. Cornehl, G. Hornung, and H. Schwarz, J. Am. Chem. Soc. **118**, 9960 (1996).
[6] U. Mazurek, D. Schröder, and H. Schwarz, Angew. Chem., Int. Ed. Engl. **41**, 2538 (2002).
[7] U. Mazurek and H. Schwarz, Chem. Commun. (Cambridge) **2003**, 1321 (2003).
[8] J. N. Harvey, D. Schröder, W. Koch, D. Danovich, S. Shaik, and H. Schwarz, Chem. Phys. Lett. **278**, 391 (1997).
[9] W. Koch and M. C. Holthausen, *A Chemist's Guide to Density Functional Theory*, 2nd ed. (Wiley-VCH, Weinheim, 2000).
[10] S. H. Vosko, L. Wilk, and M. Nusair, Can. J. Phys. **58**, 1200 (1980).
[11] A. D. Becke, Phys. Rev. A **38**, 3098 (1988).
[12] C. Lee, W. Yang, and R. G. Parr, Phys. Rev. B **37**, 785 (1988).
[13] D. Zhang, C. Zhang, and C. Liu, J. Organomet. Chem. **640**, 121 (2001).
[14] D. Zhang, C. Liu, and S. Bi, J. Phys. Chem. A **106**, 4153 (2002).
[15] Y.-C. Wang, Z.-Y. Liu, Z.-Y. Geng, X.-Y. Yang, L.-G. Gao, and X.-X. Chen, J. Mol. Struct.: THEOCHEM **765**, 27 (2006).
[16] B. J. Lynch and D. G. Truhlar, J. Phys. Chem. A **105**, 2936 (2001).
[17] X. Zhao, G. K. Koynagi, and D. K. Bohme, J. Phys. Chem. A **110**, 10607 (2006).
[18] B. J. Lynch, P. L. Fast, M. Harris, and D. G. Truhlar, J. Phys. Chem. A **104**, 4811 (2000).
[19] Y. Zhao and D. G. Truhlar, J. Phys. Chem. A **108**, 6908 (2004).
[20] A. D. Boese and J. M. L. Martin, J. Chem. Phys. **121**, 3405 (2004).
[21] S. Andersson and M. Grïning, J. Phys. Chem. A **108**, 7621 (2004).
[22] S. F. Sousa, P. A. Fernandes, and M. J. Ramos, J. Phys. Chem. A **111**, 10439 (2007).
[23] A. D. Boese, J. M. L. Martin, and N. C. Handy, J. Chem. Phys. **119**, 3005 (2003).
[24] W. J. Hehre, L. Radom, P. R. Schleyer, and J. A. Pople, *Ab Initio Molecular Orbital Theory* (Wiley, New York, 1986).
[25] R. A. Kendall, J. H. Dunning, Jr., and R. J. Harrison, J. Chem. Phys. **96**, 6796 (1992).
[26] F. Weigend, M. Haeser, H. Patzelt, and R. Ahlrichs, Chem. Phys. Lett. **294**, 143 (1998).
[27] M. Kaupp, P. R. Schleyer, H. Stoll, and H. Preuss, J. Chem. Phys. **94**, 1360 (1991).

[28] D. A. McQuarrie, *Statistical Thermodynamics* (University Science Books, Mill Valley, 1973).

[29] M. J. Frisch, G. W. Trucks, H. B. Schlegel *et al.*, GAUSSIAN 03, C.01, Gaussian, Inc., Wallingford, CT, 2004.

[30] M. Mozurkewich and S. W. Benson, J. Phys. Chem. **88**, 6429 (1984).

[31] P. J. Robinson and K. A. Holbrook, *Unimolecular Reactions* (Wiley, London, 1972).

[32] W. Forst, *Theory of Unimolecular Reactions* (Academic, New York, 1973).

[33] R. G. Gilbert and S. C. Smith, *Theory of Unimolecular and Recombination Reactions* (Blackwell Sci. Pu., Oxford, 1990).

[34] T. Baer and W. L. Hase, *Unimolecular Reaction Dynamics: Theory and Experiments* (Oxford University Press, New York, 1996).

[35] Y. Chen, A. Rauk, and E. Tschuskow-Roux, J. Phys. Chem. **95**, 9900 (1991).

[36] B. C. Garrett and D. G. Truhlar, J. Chem. Phys. **70**, 1593 (1979).

[37] X. Hu and W. L. Hase, J. Chem. Phys. **95**, 8073 (1991).

[38] J. Villá and D. G. Truhlar, Theor. Chem. Acc. **97**, 317 (1997).

[39] J. Villá, A. González-Lafont, J. M. Lluch, J. C. Corchado, and J. García-Espinosa, J. Chem. Phys. **107**, 7266 (1997).

[40] A. González-Lafont, J. M. Lluch, A. Varela-Álvarez, and J. A. Sordo, J. Phys. Chem. B **112**, 328 (2008).

[41] A. Cimas, M. Aschi, C. Barrientos, V. M. Rayón, J. A. Sordo, and A. Largo, J. Chem. Phys. **123**, 114312 (2005), and references therein.

[42] E. E. Greenwald, Y. Georgievskii, and S. J. Klippenstein, J. Phys. Chem. A **109**, 6031 (2005).

[43] Y. Georgievskii and S. J. Klippenstein, J. Chem. Phys. **122**, 194103 (2005).

[44] See EPAPS supplementary material at http://dx.doi.org/10.1063/1.3247287 for rate constants predicted by several methods at different temperatures.

[45] J. Zheng, S. Zhang, and D. G. Truhlar, J. Phys. Chem. A **112**, 11509 (2008).

[46] Y. Georgievskii and S. J. Klippenstein, J. Phys. Chem. **111**, 3802 (2007).

[47] A. Varela-Álvarez, D. Markovic, P. Vogel, and J. A. Sordo, J. Am. Chem. Soc. **131**, 9547 (2009).

[48] D. Feller and J. A. Sordo, J. Chem. Phys. **112**, 5604 (2000).

[49] D. Feller and J. A. Sordo, J. Chem. Phys. **113**, 485 (2000).

[50] J. A. Sordo, J. Chem. Phys. **114**, 1974 (2001).

[51] D. Feller, K. A. Peterson, W. A. de Jong, and D. A. Dixon, J. Chem. Phys. **118**, 3510 (2003).

[52] D. Feller, K. A. Peterson, and T. D. Crawford, J. Chem. Phys. **124**, 054107 (2006).

[53] J. Zheng, Y. Zhao, and D. G. Truhlar, J. Chem. Theory Comput. **5**, 808 (2009).

[54] D. M. Golden, J. R. Barker, and L. L. Lohr, J. Phys. Chem. A **107**, 11057 (2003).

[55] A. Maranzana, J. R. Barker, and G. Tonachini, Phys. Chem. Chem. Phys. **9**, 4129 (2007).

[56] A. Maranzana, J. R. Barker, and G. Tonachini, J. Phys. Chem. A **112**, 3666 (2008).

[57] R. S. Mulliken, J. Chem. Phys. **23**, 1833 (1955); **23**, 1841 (1955); **23**, 2338 (1955); **23**, 2343 (1955).

[58] bR. W. F. Bader, *Atoms in Molecules: A Quantum Theory* (Oxford University Press, Oxford, 1990).